iScience

CellPress

Article

Amorphous Ag_2S Micro-rods-Enhanced Fluorescence on Liquid Crystals: Cation-π Interaction-Triggered Aggregation-Induced Emission Effect

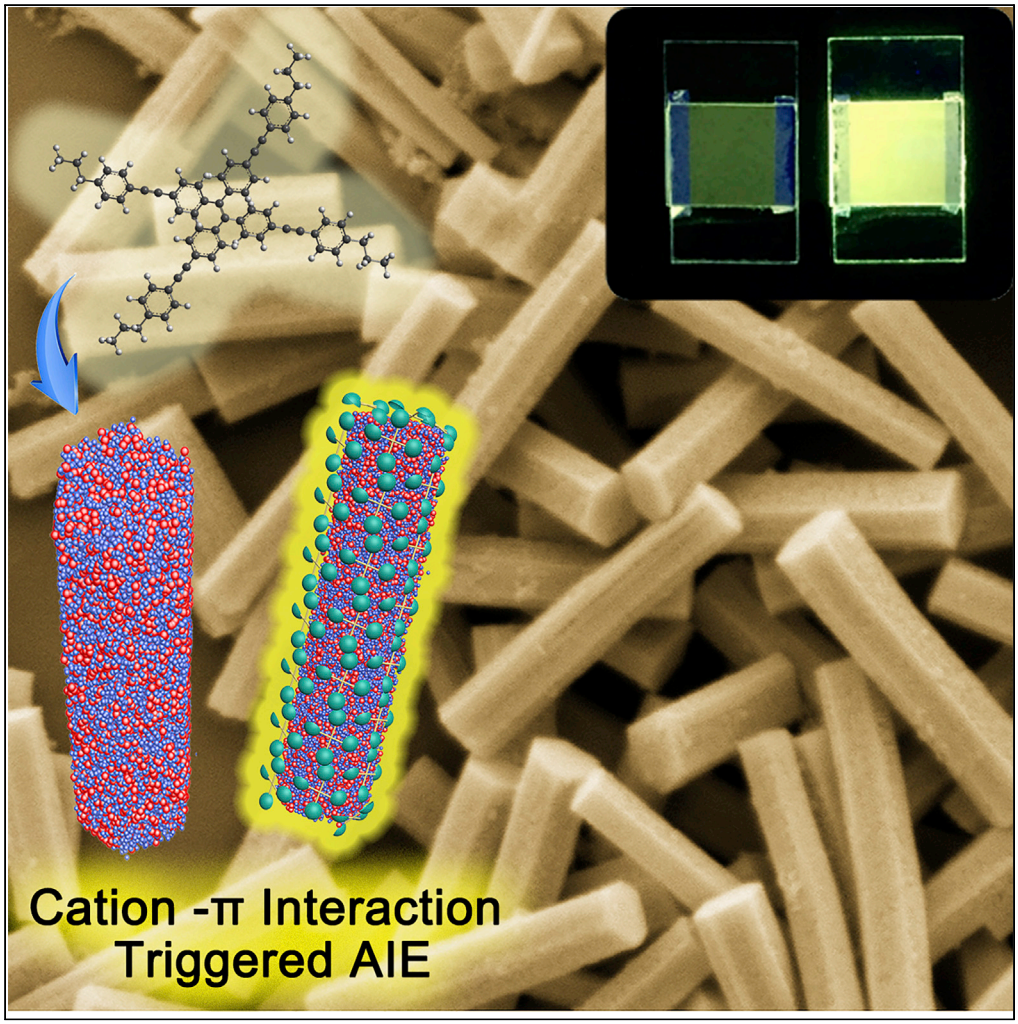

Jianxin Kang, Jian Yu, Anran Li, Dongyu Zhao, Bin Liu, Lin Guo, Benzhong Tang

zhaodongyu@buaa.edu.cn (D.Z.)
guolin@buaa.edu.cn (L.G.)
tangbenz@ust.hk (B.T.)

HIGHLIGHTS

Amorphous Ag_2S micro-rods construct additional intense interaction to trigger AIE effect

Unsaturated Ag ions and excess positive charge promote a cation-π interaction

This heterogeneous inorganic material induced a 36-fold enhancement in fluorescence

Kang et al., iScience *15*, 119–126
May 31, 2019
https://doi.org/10.1016/j.isci.2019.04.017

iScience

CellPress

Article

Amorphous Ag_2S Micro-rods-Enhanced Fluorescence on Liquid Crystals: Cation-π Interaction-Triggered Aggregation-Induced Emission Effect

Jianxin Kang,[1,4] Jian Yu,[1,4] Anran Li,[1] Dongyu Zhao,[1,*] Bin Liu,[1] Lin Guo,[1,3,*] and Benzhong Tang[2,*]

SUMMARY

Aggregation-induced emission (AIE) system has long been regarded as a promising substitute to overcome the aggregation-caused quenching in traditional luminescent liquid crystals, which could further enhance its efficiency and application. However, due to the intrinsic weak interaction between hybrid components, heterogeneous inorganic materials-induced AIE process was rarely reported. In this study, trace amounts of amorphous Ag_2S microrods and an AIE-active liquid crystalline compound tetraphenylethylene-propylbenzene (TPE-PPE) were proposed to construct additional intense interaction to trigger AIE effect. The enhanced concentration of unsaturated Ag ions and excess positive charge on Ag_2S surface promote a cation-π interaction with TPE-PPE, leading to a 36-fold increase in fluorescence, which is predominately high in luminescent liquid crystal system. To the best of our knowledge, this is the first report of the AIE process activated by cation-π interaction. This novel approach would provide guidance to fabricate high-luminescence meso phases for future luminescent display device.

INTRODUCTION

Combining intrinsic light emission and unique self-organization properties, luminescent liquid crystals (LE-LCs) have currently attracted extensive research attentions, not only for overcoming the disadvantages of conventional passive display techniques, such as low brightness and low energy efficiency, but also due to the capability of emitting linear or circular polarized light, which is of paramount importance in applications of versatile potential optoelectronic devices (Grell and Bradley, 1999; Liu et al., 2009; O'Neill and Kelly, 2003; Vijayaraghavan et al., 2008; Yuan et al., 2012). However, the luminescent performance in liquid crystalline phase has been confined by the intense intermolecular interactions among the extremely ordered LC molecules for formation of π-π stacking interactions, which would lead to intrinsic self-quenching of a majority of luminogens, described as aggregation-caused quenching (ACQ) effects (Chiang et al., 2008; Grimsdale et al., 2009; Jiang et al., 2017). Recently, a novel photophysical phenomenon of aggregation-induced emission (AIE) was discovered based on some propeller-like organic molecules (Huang et al., 2018; Li et al., 2018; Luo et al., 2001; Sugiuchi et al., 2017; Zhao et al., 2018). Instead of the normally observed quenching in "conventional" luminophores, the restriction of intramolecular motion (RIM) (Chi et al., 2012; Mao et al., 2019; Mei et al., 2015; Zhang et al., 2015b) in aggregation state would intensify their fluorescence, transforming the weakly luminescent chromo-gens into fierce luminophores. The non-traditional systems, AIE-gens, thus provided a possibility to solve the conflicts between fluorescence quenching caused by the aggregation and the requirement of self-organization for LCs, becoming promising candidates for the evolution of novel LE-LCs (Bui et al., 2016; Feng et al., 2017; Jiang et al., 2018; Kim et al., 2014; Lu et al., 2016; Park et al., 2014; Pathak et al., 2016; Tanabe et al., 2012; Yu et al., 2013).

Even though the factors influencing AIE process have been fully explored, establishing new mechanisms to trigger AIE action or a novel AIE system are still desired. For example, relative to pure organic AIE systems, research in inorganic-organic hybrid systems was still insufficient (Hu et al., 2011; Li et al., 2013; Mahtab et al., 2011; Wei et al., 2014; Zhang et al., 2014a, 2014b). As was reported, metal nanoparticles have special application in fluorescence enhancement owing to electric field effect and the induced plasmon effect (Camposeo et al., 2015; Pompa et al., 2006). With these two approaches, the emission intensities of fluorophores often show a significant increase proximal to the metallic nanostructures. However, inorganic nanoparticle-induced fluorescence enhancement governed by a more general mechanism has been rarely

[1]Key Laboratory of Bio-Inspired Smart Interfacial Science and Technology, Ministry of Education, School of Chemistry, Beihang University, Beijing 100191, P.R. China

[2]Department of Chemistry, Hong Kong University of Science and Technology, Clear Water Bay, Kowloon, Hong Kong

[3]Lead Contact

[4]These authors contributed equally

*Correspondence: zhaodongyu@buaa.edu.cn (D.Z.), guolin@buaa.edu.cn (L.G.), tangbenz@ust.hk (B.T.)

https://doi.org/10.1016/j.isci.2019.04.017

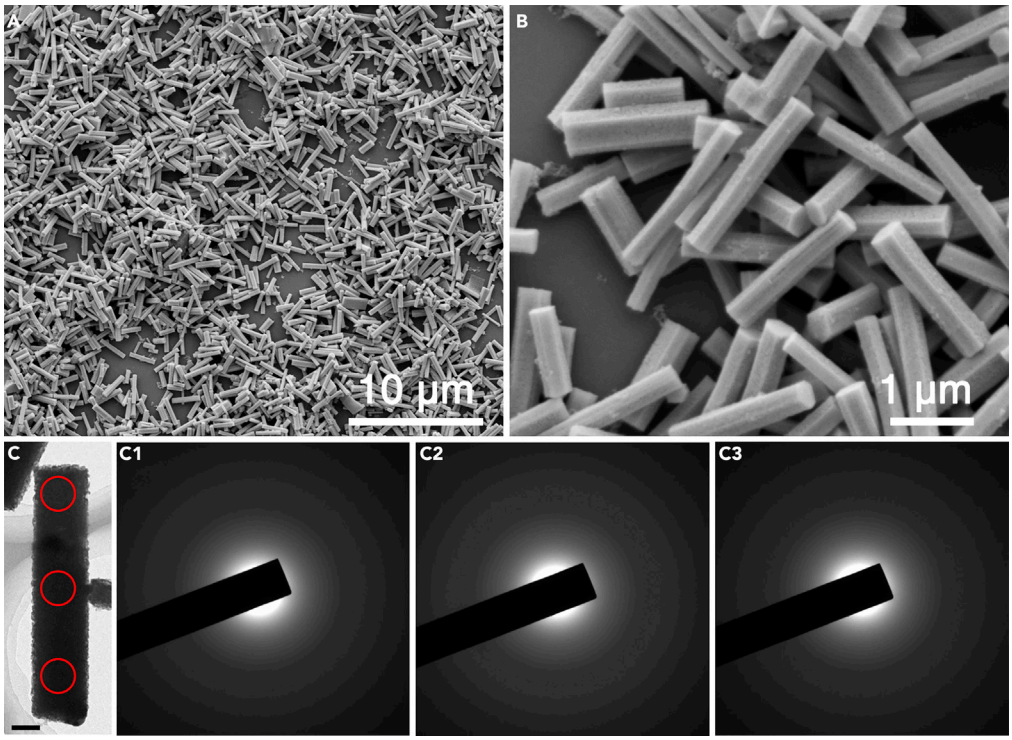

Figure 1. Morphology and Structure of Amorphous Ag_2S

(A and B) Scanning electron microscopic images of amorphous Ag_2S micro-rods under different magnification.

(C) Transmission electron microscopic images and corresponding selected area electron diffraction patterns (C_1–C_3) of the circled regions in (C). Scale bar, 100 nm in (C).

observed thus far. In inorganic nanomaterials, surface defects always provide optimal environment for reactant adsorption, which was induced by the lower coordination number than that of bulk phase (Ni and Wang, 2015; Xie et al., 2013a, 2013b). Amorphous materials that contain intrinsically disordered atomic arrangement and lower coordination number could be a potential verifiable research platform for unsaturated environment (Ye et al., 2017; Zhao et al., 2017).

In this work, we explore a novel system of invoking amorphous Ag_2S micro-rods and an AIE-active liquid crystalline compound tetraphenylethylene-propylbenzene (TPE-PPE) into the nematic LC medium to promote the enhancement of emission in LCs, by taking the advantage of cation-π interactions between the amorphous Ag_2S and the AIE-LC molecules. The S-defect-rich feature of amorphous Ag_2S micro-rod leads to enhanced surface concentration of unsaturated Ag ions and excess surface positive charge, which respectively provided adsorption sites and interaction for the adsorption of TPE-PPE. This intensive electrostatic interaction between excess cation-modified inorganic nanomaterials and conjugated electron-rich organic system restricted the intramolecular motions of TPE-PPE in the liquid crystal medium, with the synergistic combination of concentration effect leading to an ~36-fold fluorescence enhancement in LCs. Even though cation-π interaction has been universally found to be essential in molecular recognition, organic synthesis, host-guest complexation, supramolecular chemistry, and biology (Craven et al., 2016; Dougherty, 2013; Mahadevi and Sastry, 2013), to the best of our knowledge, no article concerning cation-π interaction-activated AIE process has been reported.

RESULTS

As was discussed, RIM in aggregated state is key for AIE (Hu et al., 2014; Zhang et al., 2014c, d).To provide a model with plentiful unsaturated adsorption sites, an amorphous material is synthesized through a two-step solvent precipitation and decomposition method (See Supplemental Information). As shown in Figures 1A and 1B, under different magnification of scanning electron microscope, a remarkably uniform micro-rod with clear hexagonal prism morphology was synthesized. The average diameter was ~0.3 μm,

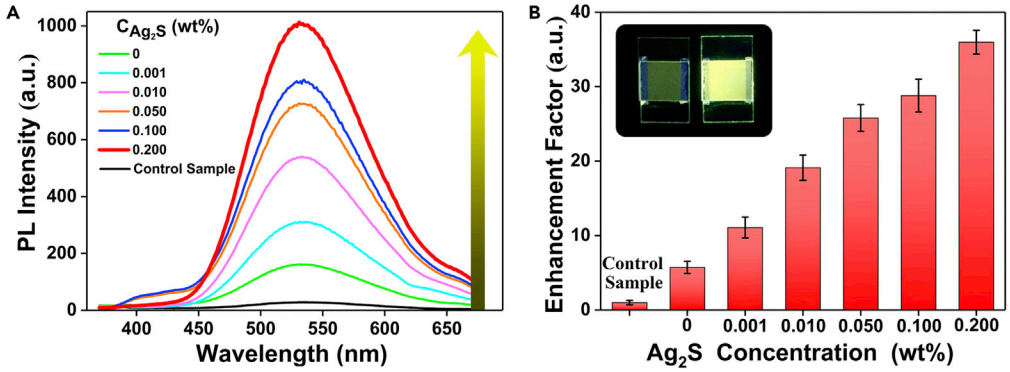

Figure 2. Amorphous Ag_2S-Enhanced Fluorescence in Luminescent Liquid Crystals

(A and B) (A) PL spectra and (B) fluorescence enhancement factor histograms of the SLC/TPE-PPE (100/0.20 wt %) with different Ag_2S concentration doping. Excitation wavelength: 340 nm. PL spectra of the control sample (100/0.01 wt %/wt %) are also shown for comparison. The inset in (B) shows photographs of control sample and the optimal sample with largest fluorescence intensity in LC cells.

and the length was ~2 μm. On the contrary, in transmission electron microscopy, the typical selected area electron diffraction patterns (Figures 1C_1–1C_3) circled in different parts of a prism show dispersive haloes, which are typical amorphous characters. X-ray diffraction pattern exhibited only a broad hump instead of sharp peaks (Figure S1), further confirming the amorphous structure.

The chemical component of this micro-rod was confirmed to be Ag_2S by X-ray photoelectron spectroscopy (XPS) in Figure S2. However, the surface atomic ratio of Ag and S exhibited by XPS was up to 6:1, much higher than the stoichiometric proportion of Ag_2S; it revealed that Ag atoms were partly enriched on the surface. To obtain more precise information, Auger electron spectroscopy (AES) was also employed, which even displayed a higher surface sensitivity than XPS (Figure S3). For Ag M4N45N45 Auger-electron line, a tiny shoulder peak at 358.3 eV emerged beside the typical Ag (I) peak at 355.8 eV (Gaarenstroom and Winograd, 1977). At the same time, the Ag M4N45N45 3P Auger-electron line was also broadened from the standard Ag (I) peak at 350.3 eV–~352.0 eV. Both of them appeared at higher kinetic energy, indicating a lower oxidation state of Ag. Combined with the higher atomic ratio of Ag and S, S atom vacancies were predicted. To judge its unsaturated environment, the S-defect was evaluated using electron paramagnetic resonance (EPR). EPR spectra provided sufficient evidences for probing sulfur vacancies with obvious signals at 320–324 mT, which were identified as electrons trapped on sulfur vacancies (Figure S4). Sulfur vacancy-induced excess surface positive charge was also detected by zeta potential, whose corresponding result showed a large positive as high as 45 $\pm$ 4 mV (Figure S5), indicating plentiful positive charges. The enhanced surface concentration of unsaturated Ag ions and excess positive charge on the surface made it a potential platform for molecular connection and electric charge transformation.

Then, the luminescent LC systems composed of the LC host, an AIE-active luminogen, and amorphous Ag_2S were fabricated and evaluated through photoluminescence (PL) spectroscopy. Here, the positive LC is nematic LC, SLC1717, and the AIE-LC was TPE-PPE (Zhao et al., 2015, 2016), whose molecular structure is shown in Figure S6. As shown in Figure S7, the homogeneous micrographs of polarization microscope exhibited that the alignment of LCs was not disturbed in the presence of Ag_2S at the concentration of 0.2 wt %. The intrinsic AIE effect was first studied, in which 0.20 wt % TPE-PPE led to approximately 5.70-fold higher optimal emission intensity than 0.01 wt % compositions (Figures S8A and S8A′). Fixing the optimal concentration of TPE-PPE at 0.20 wt %, PL measurements on varying concentrations of amorphous Ag_2S displayed a maximum PL intensity at an Ag_2S concentration of 0.20 wt %, with 6-fold enhancement (Figure 2A). It was an exciting 36-fold enhancement than the primal control sample with 0.01 wt % TPE-PPE compositions as shown in Figure 2B. Apart from the PL spectroscopy, the quantum yield of the system also exhibited the same tendency as PL intensity, which was enhanced along with the increase of Ag_2S doping (Table S1). This aggregation-induced enhancement was attributed to the intensive interaction of amorphous Ag_2S and AIE-gens, because the large enhancement could also be repeated in glycerinum-tetrahydrofuran (v/v 1:1) solvent (Figure S9). Moreover, the fluorescence stability of the composites was also evaluated by monitoring the changes in PL intensity. Under ambient conditions, the LC

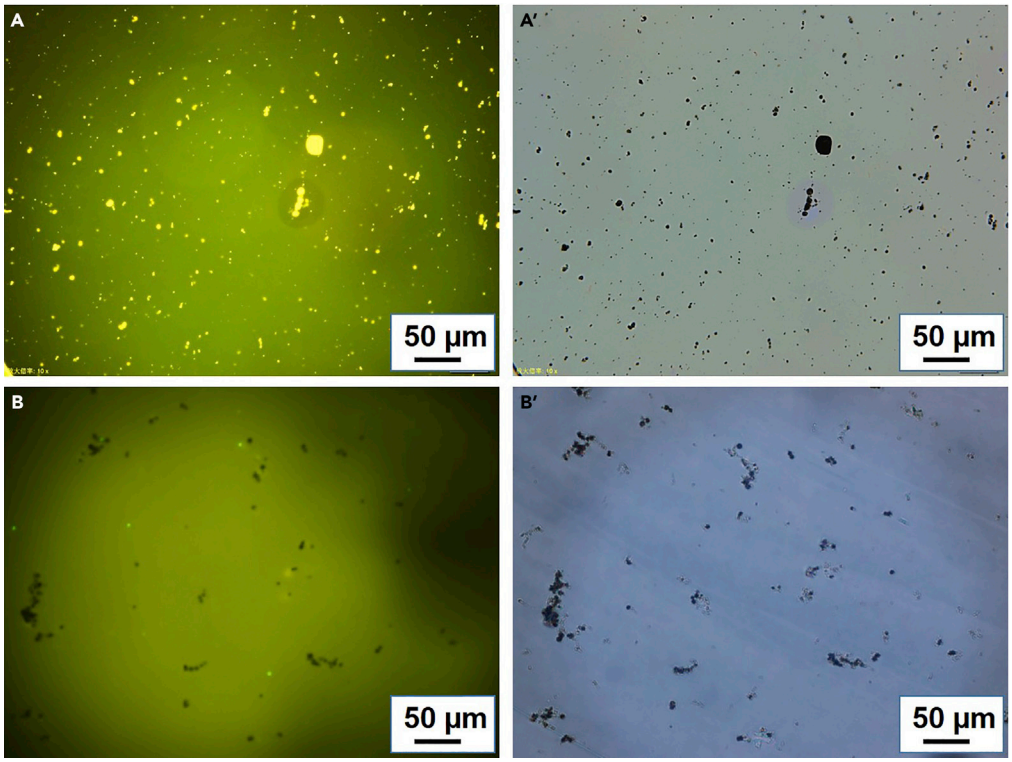

Figure 3. Comparison of Ag_2S Induced AIE and ACQ under Fluorescence Microscope

(A and A′) Photographs of the LC test cell filled with LC-Ag_2S-TPE-PPE.

(B and B′): Photographs of the LC test cell filled with LC-Ag_2S-fluorescein. (A and B) Images were taken under fluorescence microscope.

cells were found to be quite stable for at least 1 month and almost no variations were observed in PL performance. This result was fascinating when compared with ACQ effects in fluorescein (Figures S8B and S8B′), in which the rigid planar aromatic structure (Figure S10) would lead to π-π stacking interaction in LC phase aggregation. As was compared, if Ag_2S was added into the SLC1717/fluorescein composite (Figure S11), its emission is significantly quenched.

Till now, studies on inorganic-organic hybrid systems regarding fluorescence enhancement are insufficient (Hu et al., 2011; Xu et al., 2011). To reveal the mechanism of Ag_2S-induced fluorescence enhancement, the fluorescent performances of LCs-TPE-PPE-Ag_2S and the LCs-fluorescein-Ag_2S systems were compared using fluorescence microscope. As shown in Figures 3A and 3A′, the LC cell composed of LCs-Ag_2S-TPE-PPE was observed to be light emitting and the Ag_2S micro-rods doped in it exhibited higher brightness than the luminescent LC host. In contrast, the Ag_2S micro-rods doped in the LCs-Ag_2S-fluorescein system were dimmer than the light-emitting LCs as, shown in Figures 3B and 3B′. Therefore the fluorescence enhancement should be attributed to the adsorption of AIE-active TPE-PPE to the doped Ag_2S. Once dispersed into the LC medium, Ag_2S micro-rods would absorb fluorescent dyes and lead to the second aggregation of fluorescent dye in local environment, which further enhanced the emission of luminescent LC mixtures.

For amorphous inorganic nanomaterials, surface defects always provide optimal environment for reactant adsorption (Zhang et al., 2015a). In our system, the sulfur vacancies of amorphous Ag_2S would induce unsaturated coordinated structure, which would be an appropriate environment for TPE-PPE abortion, while positive charges coming from the surplus Ag would also afford the electron environment (Craven et al., 2016) for the link of π-electron circulation of TPE-PPE. To confirm the interaction, the amorphous Ag_2S micro-rod was compared with crystal Ag and $AgNO_3$ nanoparticles under the same modified condition by AES spectra (Figure S12). It was clear that Auger-electron line of Ag(I) parts of TPE-PPE-modified amorphous Ag_2S micro-rods exhibited a tiny shift to the high kinetic energy. It means the conjugate electrons of

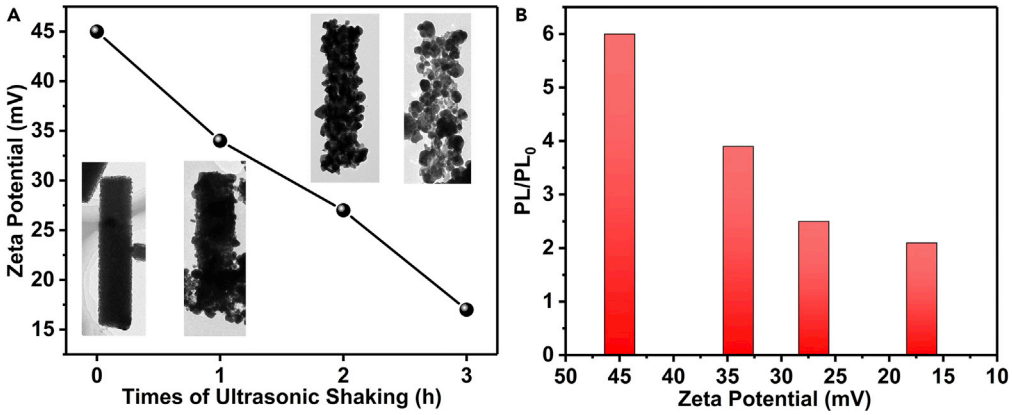

Figure 4. The Corresponding Relation of Ag_2S Crystallinity, Zeta Potential, and Fluorescence Intensity

(A) The zeta potential and corresponding morphology evolution along with crystalline process induced by ultrasonic shaking.

(B) Relative fluorescence intensity of LC cells filled with emissive LC composites against the zeta potential of Ag_2S. Emissive LC composite = LC1717 + 0.2 wt % TPE-PPE + 0.2 wt % processed Ag_2S. Here, the LC cell filled with 0.2 wt % TPE-LC1717 was used as a standard (PL_0) sample.

TPE-PPE indeed partly transferred to the surficial Ag(I) ions, leading to a lower oxidation state and a lower binding energy of Ag(I). In contrast, crystal Ag and $AgNO_3$ showed almost the same spectra with their modified samples, and it was also embodied in their PL spectra, which displayed a maximum enhancement of PL intensity of about 1.7 times (Figure S13).

Thus the amorphous Ag_2S micro-rods could be an excellent second-level assembly core to absorb TPE-PPE. To confirm that the amorphous structure induced surface positive electric charge, a series of materials with different crystallinities was prepared through long-time ultrasonic shaking. After 3-h treatment, the amorphous micro-rods would turn to hollow crystal Ag_2S rods, which were assembled by abundant 50- to 100-nm nanospheres (Figure S14). Products of different stage were measured by zeta potential to quantificationally evaluate the electric charge on the surface. It is clear that along with the crystallization process, zeta potential persistently reduces from ~45 mV to ~15 mV, illustrating the fading away of surface positive electric charges (Figure 4A). Then the corresponding fluorescence intensity (PL/PL_0) of the LCs-TPE-PPE-Ag_2S composites with different degrees of crystallinity of Ag_2S was monitored (Figure 4B). The relative fluorescence intensity exhibits a gradual increase with the increase of the zeta potential of the Ag_2S, revealing the essential role of surface electric charges of doped Ag_2S on the fluorescence activities of TPE-PPE. To verify the interaction between surface positive charge and conjugated electron-rich aromatic system, a rough model was established to evaluate the single point energies of Ag atom, Ag (I) ion, Ag_2S cluster, and phenyl using the first principles calculation method (Table S1). When coupled with the phenyl ring, the binding energies were calculated to increase along with the increase of the electric charge (Figure S15). Evidently, this calculation result suggests that the existence of cation-π interactions played the dominant role between inorganic materials and conjugated electron-rich TPE-PPE.

DISCUSSION

Based on our experimental and calculation results, a proposed mechanism for amorphous Ag_2S micro-rods-induced emission enhancement of AIE-LC system has been extracted (Scheme 1). The employed amorphous Ag_2S will absorb the fluorescent dyes (TPE-PPE) in the LC medium, leading to the aggregation of the AIE-gen; it was attributed to the enhanced surface concentration of unsaturated Ag ions and excess positive charge on the surface of the amorphous Ag_2S micro-rods, which, respectively, provided optimized adsorption sites and adsorption interaction, and promoted surface Ag ions to form cation-π interaction with fluorescence dyes containing conjugated π-electrons. As a result, the RIM process was triggered and strong emission was turned on. On the contrary, when the amorphous Ag_2S was doped into LC-fluorescein system, the fluorescence was quenched, owing to the similar cation-π interaction between Ag_2S and aromatic rings of fluorescence.

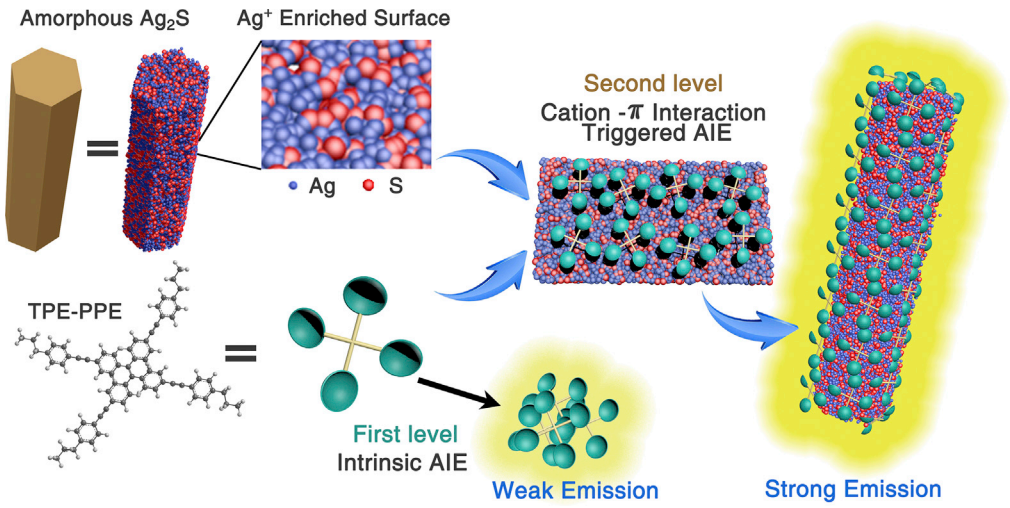

Scheme 1. Schematic Illustration of Proposed Mechanism for Amorphous Ag_2S-Induced AIE Behavior through Ag-π Interaction between Ag_2S Surface and TPE-PPE

In summary, novel amorphous Ag_2S micro-rods were synthesized to be a potential aggregation center to explore if inorganic nanoparticles improved the luminescence properties of AIE-active LCs. With trace amounts of amorphous Ag_2S and AIE dye TPE-PPE introduced into nematic LCs, an ~36-fold PL intensity enhancement was obtained. To the best of our knowledge, the enhancement factor is predominately high among those reported for luminescent LCs. The intensive electrostatic interaction between excess cation of amorphous inorganic nanomaterials and conjugated electron-rich organic system played a dominant role in the emission enhancement of TPE-PPE in the nematic LC host. Extraordinarily, it is the first report to applying cation-π interaction into the fluorescence enhancement of LC systems. This report will contribute to open up a new prospect of light-emitting LCs by introducing micro-materials into LC systems, leading to more potential applications for fabricating LC dispalys.

Limitations of the Study

We showed the intense interaction between amorphous Ag_2S micro-rods and the AIE dye TPE-PPE through the obvious luminescence enhancement under fluorescence microscope. However, it is very difficult to simulate this process. Even though the atomic-level model built in this work is able to give a qualitative description to evaluate the cation-π interaction, a more perfect model is needed in the future for a better understanding.

METHODS

All methods can be found in the accompanying Transparent Methods supplemental file.

SUPPLEMENTAL INFORMATION

Supplemental Information can be found online at https://doi.org/10.1016/j.isci.2019.04.017.

ACKNOWLEDGMENTS

This work was supported by the National Natural Science Foundation of China (51673008, 51532001, 21471013), the National Key R&D Program of China (2018YFB0703703), the Beijing Natural Science Foundation (2194077, 2192030), the National Postdoctoral Program for Innovative Talents (BX20180020), and the China Postdoctoral Science Foundation Funded Project (2018M640041).

AUTHOR CONTRIBUTIONS

Conceptualization, L.G. and B.T.; Methodology, J.K., and D.Z.; Investigation, J.K., J.Y., A.L., B.L., and D.Z.; Writing – Original Draft, J.K. and D.Z.; Writing –Review & Editing, L.G. and B.T.

DECLARATION OF INTERESTS

The authors declare no competing interests.

Received: December 15, 2018
Revised: March 14, 2019
Accepted: March 26, 2019
Published: May 31, 2019

REFERENCES

Bui, H.T., Kim, J., Kim, H.-J., Cho, B.-K., and Cho, S. (2016). Advantages of mobile liquid-crystal phase of AIE luminogens for effective solid-state emission. J. Phys. Chem. C *120*, 26695–26702.

Camposeo, A., Persano, L., Manco, R., Wang, Y., Del Carro, P., Zhang, C., Li, Z.-Y., Pisignano, D., and Xia, Y. (2015). Metal-enhanced near-infrared fluorescence by micropatterned gold nanocages. ACS Nano *9*, 10047–10054.

Chi, Z., Zhang, X., Xu, B., Zhou, X., Ma, C., Zhang, Y., Liu, S., and Xu, J. (2012). Recent advances in organic mechanofluorochromic materials. Chem. Soc. Rev. *41*, 3878–3896.

Chiang, C.-L., Tseng, S.-M., Chen, C.-T., Hsu, C.-P., and Shu, C.-F. (2008). Influence of molecular dipoles on the photoluminescence and electroluminescence of dipolar spirobifluorenes. Adv. Funct. Mater. *18*, 248–257.

Craven, T.W., Cho, M.-K., Traaseth, N.J., Bonneau, R., and Kirshenbaum, K. (2016). A miniature protein stabilized by a cation–π interaction network. J. Am. Chem. Soc. *138*, 1543–1550.

Dougherty, D.A. (2013). The Cation–π interaction. Acc. Chem. Res. *46*, 885–893.

Feng, C., Ding, Y.-H., Han, X.-D., Yu, W.-H., Xiang, S.-K., Wang, B.-Q., Hu, P., Li, L.-C., Chen, X.-Z., and Zhao, K.-Q. (2017). Triphenylene 2, 3-dicarboxylic imides as luminescent liquid crystals: mesomorphism, optical and electronic properties. Dyes Pigments *139*, 87–96.

Gaarenstroom, S.W., and Winograd, N. (1977). Initial and final state effects in the ESCA spectra of cadmium and silver oxides. J. Chem. Phys. *67*, 3500–3506.

Grell, M., and Bradley, D.D.C. (1999). Polarized luminescence from oriented molecular materials. Adv. Mater. *11*, 895–905.

Grimsdale, A.C., Leok Chan, K., Martin, R.E., Jokisz, P.G., and Holmes, A.B. (2009). Synthesis of light-emitting conjugated polymers for applications in electroluminescent devices. Chem. Rev. *109*, 897–1091.

Hu, R., Leung, N.L.C., and Tang, B.Z. (2014). AIE macromolecules: syntheses, structures and functionalities. Chem. Soc. Rev. *43*, 4494–4562.

Hu, X.-M., Chen, Q., Zhou, D., Cao, J., He, Y.-J., and Han, B.-H. (2011). One-step preparation of fluorescent inorganic–organic hybrid material used for explosive sensing. Polym. Chem. *2*, 1124–1128.

Huang, H., Liu, M., Wan, Q., Jiang, R., Xu, D., Huang, Q., Wen, Y., Deng, F., Zhang, X., and Wei, Y. (2018). Facile fabrication of luminescent hyaluronic acid with aggregation-induced emission through formation of dynamic bonds and their theranostic applications. Mater. Sci. Eng. C Mater. Biol. Appl. *91*, 201–207.

Jiang, R., Liu, H., Liu, M., Tian, J., Huang, Q., Huang, H., Wen, Y., Cao, Q.-y., Zhang, X., and Wei, Y. (2017). A facile one-pot Mannich reaction for the construction of fluorescent polymeric nanoparticles with aggregation-induced emission feature and their biological imaging. Mater. Sci. Eng. C Mater. Biol. Appl. *81*, 416–421.

Jiang, R., Liu, M., Chen, T., Huang, H., Huang, Q., Tian, J., Wen, Y., Cao, Q.-y., Zhang, X., and Wei, Y. (2018). Facile construction and biological imaging of cross-linked fluorescent organic nanoparticles with aggregation-induced emission feature through a catalyst-free azide-alkyne click reaction. Dyes Pigments *148*, 52–60.

Kim, J., Cho, S., and Cho, B.-K. (2014). An unusual stacking transformation in liquid-crystalline columnar assemblies of clicked molecular propellers with tunable light emissions. Chem. Eur. J. *20*, 12734–12739.

Li, J.-A., Zhou, J., Mao, Z., Xie, Z., Yang, Z., Xu, B., Liu, C., Chen, X., Ren, D., Pan, H., et al. (2018). Transient and persistent room-temperature mechanoluminescence from a white-light-emitting AIEgen with tricolor emission switching triggered by light. Angew. Chem. Int. Ed. *130*, 6559–6563.

Li, M., Lam, J.W.Y., Mahtab, F., Chen, S., Zhang, W., Hong, Y., Xiong, J., Zheng, Q., and Tang, B.Z. (2013). Biotin-decorated fluorescent silica nanoparticles with aggregation-induced emission characteristics: fabrication, cytotoxicity and biological applications. J. Mater. Chem. B *1*, 676–684.

Liu, J., Lam, J.W.Y., and Tang, B.Z. (2009). Acetylenic polymers: syntheses, structures, and functions. Chem. Rev. *109*, 5799–5867.

Lu, H., Zhang, C., Xia, G., Wu, S., Zhang, G., Yang, J., and Qiu, L. (2016). Continuously tunable emission color based on the molecular aggregation of (2Z,2′Z)-2,2′-(1,4-phenylenae) bis(3-(4-(dodecyloxy)phenyl)acrylonitrile). RSC Adv. *6*, 96196–96201.

Luo, J., Xie, Z., Lam, J.W.Y., Cheng, L., Chen, H., Qiu, C., Kwok, H.S., Zhan, X., Liu, Y., Zhu, D., et al. (2001). Aggregation-induced emission of 1-methyl-1,2,3,4,5-pentaphenylsilole. Chem. Commun. 1740–1741.

Mahadevi, A.S., and Sastry, G.N. (2013). Cation–π interaction: its role and relevance in chemistry, biology, and material science. Chem. Rev. *113*, 2100–2138.

Mahtab, F., Yu, Y., Lam, J.W.Y., Liu, J., Zhang, B., Lu, P., Zhang, X., and Tang, B.Z. (2011). Fabrication of silica nanoparticles with both efficient fluorescence and strong magnetization and exploration of their biological applications. Adv. Funct. Mater. *21*, 1733–1740.

Mao, L., Liu, Y., Yang, S., Li, Y., Zhang, X., and Wei, Y. (2019). Recent advances and progress of fluorescent bio-/chemosensors based on aggregation-induced emission molecules. Dyes Pigments *162*, 611–623.

Mei, J., Leung, N.L.C., Kwok, R.T.K., Lam, J.W.Y., and Tang, B.Z. (2015). Aggregation-induced emission: together we shine, united we soar! Chem. Rev. *115*, 11718–11940.

Ni, B., and Wang, X. (2015). Face the edges: catalytic active sites of nanomaterials. Adv. Sci. *2*, 1500085.

O'Neill, M., and Kelly, S.M. (2003). Liquid crystals for charge transport, luminescence, and photonics. Adv. Mater. *15*, 1135–1146.

Park, J.W., Nagano, S., Yoon, S.-J., Dohi, T., Seo, J., Seki, T., and Park, S.Y. (2014). High contrast fluorescence patterning in cyanostilbene-based crystalline thin films: crystallization-induced mass flow via a photo-triggered phase transition. Adv. Mater. *26*, 1354–1359.

Pathak, S.K., Pradhan, B., Gupta, M., Pal, S.K., and Sudhakar, A.A. (2016). Liquid-crystalline star-shaped supergelator exhibiting aggregation-induced blue light emission. Langmuir *32*, 9301–9312.

Pompa, P.P., Martiradonna, L., Torre, A.D., Sala, F.D., Manna, L., De Vittorio, M., Calabi, F., Cingolani, R., and Rinaldi, R. (2006). Metal-enhanced fluorescence of colloidal nanocrystals with nanoscale control. Nat. Nanotechnol. *1*, 126–130.

Sugiuchi, M., Maeba, J., Okubo, N., Iwamura, M., Nozaki, K., and Konishi, K. (2017). Aggregation-induced fluorescence-to-phosphorescence switching of molecular gold clusters. J. Am. Chem. Soc. *139*, 17731–17734.

Tanabe, K., Suzui, Y., Hasegawa, M., and Kato, T. (2012). Full-color tunable photoluminescent ionic liquid crystals based on tripodal pyridinium, pyrimidinium, and quinolinium salts. J. Am. Chem. Soc. *134*, 5652–5661.

Vijayaraghavan, R.K., Abraham, S., Akiyama, H., Furumi, S., Tamaoki, N., and Das, S. (2008). Photoresponsive glass-forming butadiene-based chiral liquid crystals with circularly polarized photoluminescence. Adv. Funct. Mater. *18*, 2510–2517.

Wei, Z., Gu, Z.-Y., Arvapally, R.K., Chen, Y.-P., McDougald, R.N., Ivy, J.F., Yakovenko, A.A., Feng, D., Omary, M.A., and Zhou, H.-C. (2014). Rigidifying fluorescent linkers by metal–organic framework formation for fluorescence blue shift and quantum yield enhancement. J. Am. Chem. Soc. *136*, 8269–8276.

Xie, J., Zhang, H., Li, S., Wang, R., Sun, X., Zhou, M., Zhou, J., Lou, X.W., and Xie, Y. (2013a). Defect-rich MoS2 ultrathin nanosheets with additional active edge sites for enhanced electrocatalytic hydrogen evolution. Adv. Mater. *25*, 5807–5813.

Xie, J., Zhang, J., Li, S., Grote, F., Zhang, X., Zhang, H., Wang, R., Lei, Y., Pan, B., and Xie, Y. (2013b). Controllable disorder engineering in oxygen-incorporated MoS2 ultrathin nanosheets for efficient hydrogen evolution. J. Am. Chem. Soc. *135*, 17881–17888.

Xu, Y., Chen, L., Guo, Z., Nagai, A., and Jiang, D. (2011). Light-emitting conjugated polymers with microporous network architecture: interweaving scaffold promotes electronic conjugation, facilitates exciton migration, and improves luminescence. J. Am. Chem. Soc. *133*, 17622–17625.

Ye, H., Ma, L., Zhou, Y., Wang, L., Han, N., Zhao, F., Deng, J., Wu, T., Li, Y., and Lu, J. (2017). Amorphous MoS_3 as the sulfur-equivalent cathode material for room-temperature Li–S and Na–S batteries. Proc. Natl. Acad. Sci. U S A *114*, 13091–13096.

Yu, W.-H., Chen, C., Hu, P., Wang, B.-Q., Redshaw, C., and Zhao, K.-Q. (2013). Tetraphenylethene–triphenylene oligomers with an aggregation-induced emission effect and discotic columnar mesophase. RSC Adv. *3*, 14099–14105.

Yuan, W.Z., Yu, Z.-Q., Lu, P., Deng, C., Lam, J.W.Y., Wang, Z., Chen, E.-Q., Ma, Y., and Tang, B.Z. (2012). High efficiency luminescent liquid crystal: aggregation-induced emission strategy and biaxially oriented mesomorphic structure. J. Mater. Chem. *22*, 3323–3326.

Zhang, M., Feng, G., Song, Z., Zhou, Y.-P., Chao, H.-Y., Yuan, D., Tan, T.T.Y., Guo, Z., Hu, Z., Tang, B.Z., et al. (2014a). Two-dimensional metal–organic framework with wide channels and responsive turn-on fluorescence for the chemical sensing of volatile organic compounds. J. Am. Chem. Soc. *136*, 7241–7244.

Zhang, X., Meng, F., Mao, S., Ding, Q., Shearer, M.J., Faber, M.S., Chen, J., Hamers, R.J., and Jin, S. (2015a). Amorphous MoSxCly electrocatalyst supported by vertical graphene for efficient electrochemical and photoelectrochemical hydrogen generation. Energ. Environ. Sci. *8*, 862–868.

Zhang, X., Wang, K., Liu, M., Zhang, X., Tao, L., Chen, Y., and Wei, Y. (2015b). Polymeric AIE-based nanoprobes for biomedical applications: recent advances and perspectives. Nanoscale *7*, 11486–11508.

Zhang, X., Zhang, X., Yang, B., Liu, L., Hui, J., Liu, M., Chen, Y., and Wei, Y. (2014b). Aggregation-induced emission dye based luminescent silica nanoparticles: facile preparation, biocompatibility evaluation and cell imaging applications. RSC Adv. *4*, 10060–10066.

Zhang, X., Zhang, X., Yang, B., Liu, M., Liu, W., Chen, Y., and Wei, Y. (2014c). Fabrication of aggregation induced emission dye-based fluorescent organic nanoparticles via emulsion polymerization and their cell imaging applications. Polym. Chem. *5*, 399–404.

Zhang, X., Zhang, X., Yang, B., Liu, M., Liu, W., Chen, Y., and Wei, Y. (2014d). Polymerizable aggregation-induced emission dye-based fluorescent nanoparticles for cell imaging applications. Polym. Chem. *5*, 356–360.

Zhao, D., Fan, F., Cheng, J., Zhang, Y., Wong, K.S., Chigrinov, V.G., Kwok, H.S., Guo, L., and Tang, B.Z. (2015). Light-emitting liquid crystal displays based on an aggregation-induced emission luminogen. Adv. Opt. Mater. *3*, 199–202.

Zhao, D., He, H., Gu, X., Guo, L., Wong, K.S., Lam, J.W.Y., and Tang, B.Z. (2016). Circularly polarized luminescence and a reflective photoluminescent chiral nematic liquid crystal display based on an aggregation-induced emission luminogen. Adv. Opt. Mater. *4*, 534–539.

Zhao, H., Zhu, Y., Li, F., Hao, R., Wang, S., and Guo, L. (2017). A generalized strategy for the synthesis of large-size ultrathin two-dimensional metal oxide nanosheets. Angew. Chem. Int. Ed. *56*, 8766–8770.

Zhao, Z., Gao, S., Zheng, X., Zhang, P., Wu, W., Kwok, R.T.K., Xiong, Y., Leung, N.L.C., Chen, Y., Gao, X., et al. (2018). Rational design of perylenediimide-substituted triphenylethylene to electron transporting aggregation-induced emission luminogens (aiegens) with high mobility and near-infrared emission. Adv. Funct. Mater. *28*, 1705609.

ISCI, Volume *15*

Supplemental Information

Amorphous Ag_2S Micro-rods-Enhanced Fluorescence on Liquid Crystals: Cation-π Interaction-Triggered Aggregation-Induced Emission Effect

Jianxin Kang, Jian Yu, Anran Li, Dongyu Zhao, Bin Liu, Lin Guo, and Benzhong Tang

Supporting Information

Amorphous Ag_2S Microrods Enhanced Fluorescence on Luminescent Liquid Crystals: Cation-π Interaction Triggered AIE Effect

Jianxin Kang, [1,4] Jian Yu, [1,4] Anran Li, [1] Dongyu Zhao, [1,*] Bin Liu[1], Lin Guo, [1,3,*] and Benzhong Tang[2,*]

[1] Beijing Advanced Innovation Center for Biomedical Engineering，School of Chemistry, Beihang University, Beijing 100191, P.R. China
[2] Department of Chemistry, Hong Kong University of Science and Technology, Clear Water Bay, Kowloon, Hong Kong
[3] Lead Contact
[4] These authors contributed equally to this work.
*Correspondence: guolin@buaa.edu.cn

This PDF files includes:

Supplemental Figures

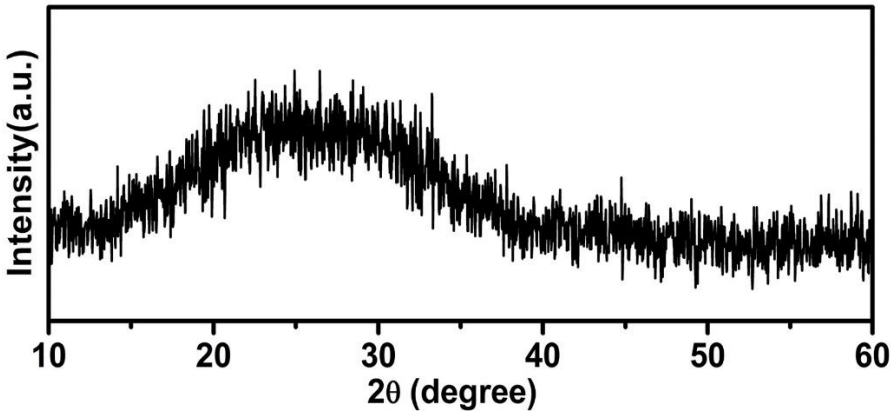

Figure S1. XRD pattern of amorphous Ag_2S micro-rods, related to Figure 1. It exhibited only a broad hump instead of sharp peaks, further confirmed the amorphous structure.

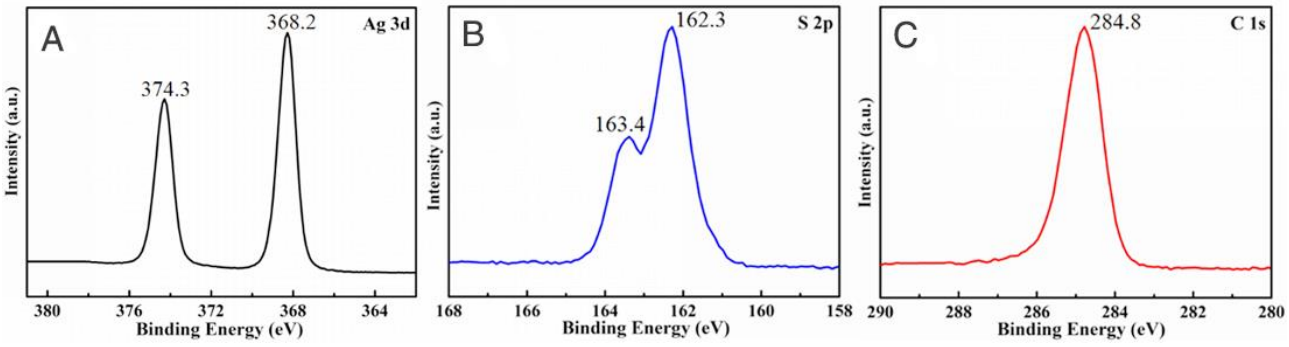

Figure S2. XPS spectra of (A) Ag 3d, (B) S 2p and (C) C 1s for amorphous Ag_2S micro-rods, related to Figure 1. The Ag $3d_{5/2}$ and Ag $3d_{3/2}$ binding energies were located at 368.2 eV and 374.3 eV respectively, which indicates the Ag (I) species. While, the S $2p_{3/2}$ and S $2p_{1/2}$ peaks appeared at 162.3 eV and 163.5 eV, respectively, a typical inorganic covalent bond environment for S. C 1s spectrum was used for calibration. Thus, the as-prepared micro-rods should be amorphous Ag_2S.

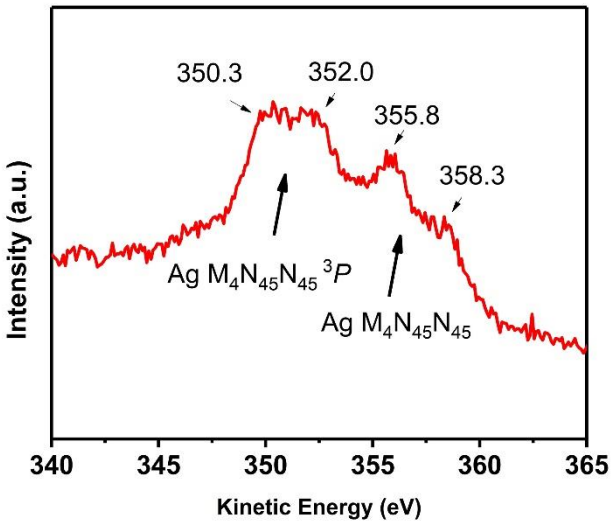

Figure S3. AES spectra of Ag $M_4N_{45}N_{45}$ Auger-electron line for amorphous Ag_2S micro-rods, related to Figure 1. A tiny shoulder peak at 358.3 eV was emerged beside the typical Ag (I) peak at 355.8 eV. At the same time， the Ag $M_4N_{45}N_{45}$ ^3P Auger-electron line was also broadened from the standard Ag (I) peak at 350.3 eV to ~352.0 eV. Both appeared at higher kinetic energy, indicated a lower oxidation state of Ag.

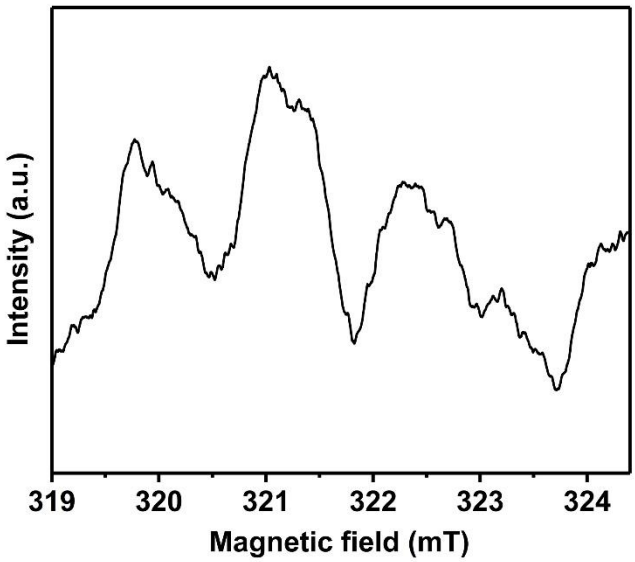

Figure S4. Electron paramagnetic resonance (EPR) spectra of amorphous Ag_2S micro-rods, related to Figure 1. EPR spectra provided sufficient evidences for probing sulfur vacancies with obvious signals at about 319~324 mT, which were identified as electrons trapped on sulfur vacancies.

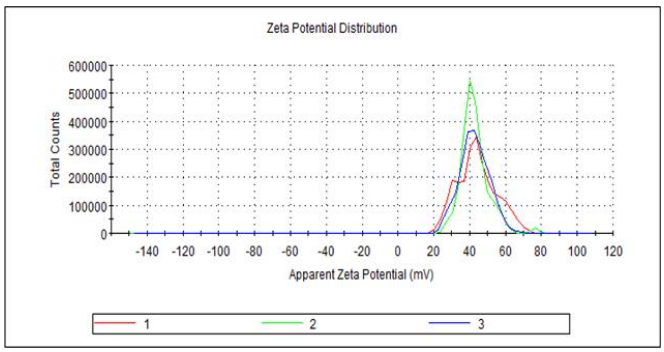

Figure S5. Zeta potential distribution of amorphous Ag_2S micro-rods dispersed in deionized water, whose corresponded result showed a large positive as high as 45±4 mV (three independent experiments showed in three different colors), indicating a plentiful of positive charge, related to Figure 1.

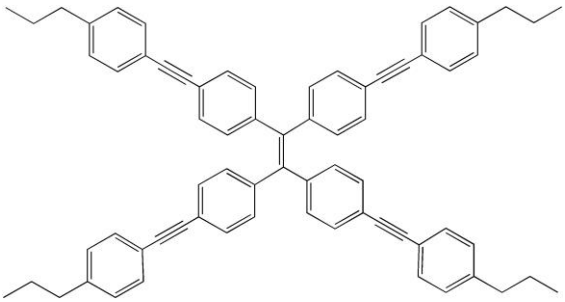

Figure S6. The chemical structure of TPE-PPE, related to Figure 2. In this molecule, it has a conjugation structure of four mesogenic units and a TPE core, exhibiting both AIE behaviors and liquid crystalline properties. Four mesogenic units are linked to a central olefin stator through single-bond axes, respectively.

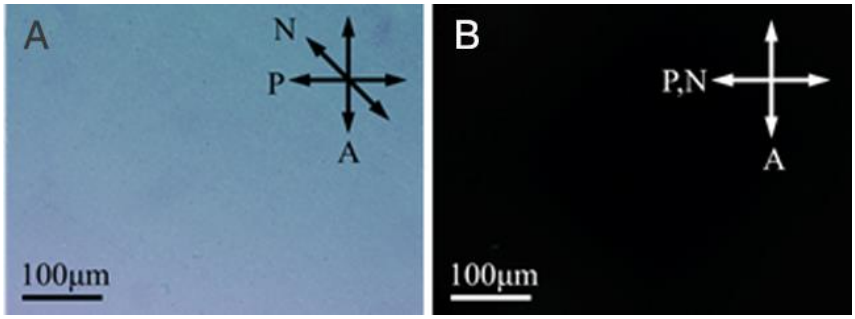

Figure S7. POM micrographs of the LC/TPE-PPE/Ag_2S (0.20 wt%) composite with N at (a) 45° and (b) 0° to P, related to Figure 2. (A: analyzer, P: polarizer, N: director of LCs).

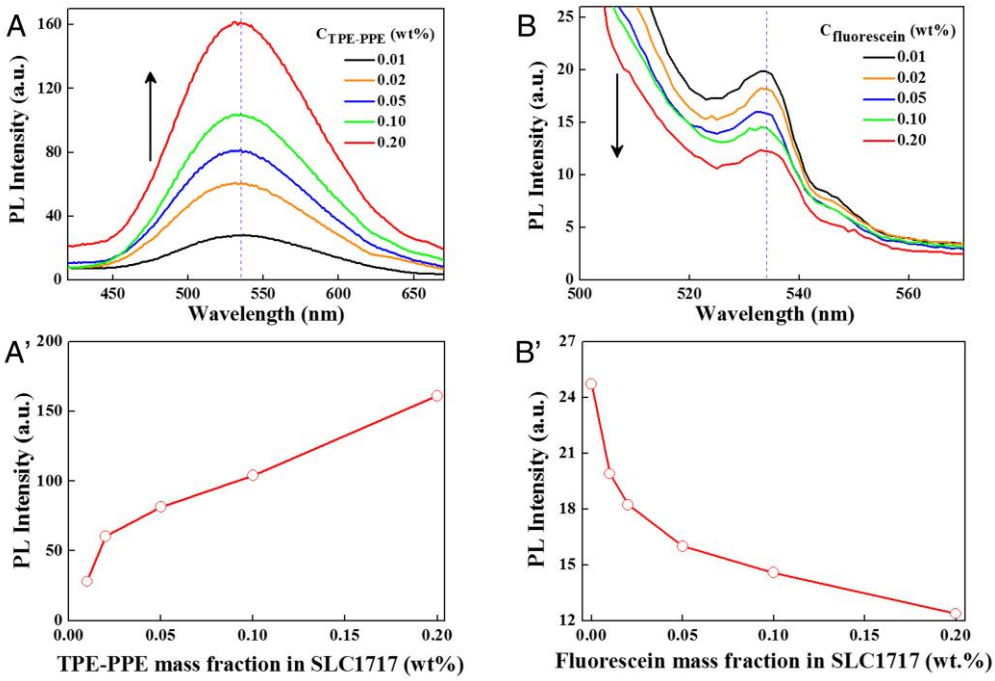

Figure S8, related to Figure 2 and 3**.** (A) Normal PL spectra of the LC cells composed of nematic SLC1717 and TPE-PPE with different concentrations. Excitation wavelength: 340 nm. (A') PL intensity values at ~535 nm versus the concentrations of TPE-PPE in SLC1717. (B) PL spectra of the LC cells composed of SLC1717 and fluorescein with the identical concentrations. Excitation wavelength: 489 nm. (B') PL intensity values at ~535 nm versus the concentrations of fluorescein in in SLC1717. It is worthy to notice that LCs containing various concentrations of TPE-PPE exhibited identical emission profile and wavelength (λ_{max} = 535 nm), excited by 340 nm ultraviolet light. Distinctly, it can be observed that all the luminescent liquid crystal samples displayed a fairly broad PL spectrum in the visible regions from 450 nm to 650 nm. Moreover, the fluorescence behavior varied directly with concentration of TPE-PPE in LC phases. The emission of the LC host dissolved with 0.01 wt% TPE-PPE was so faint that its PL spectra appeared a dinky peak. However, the emission of the "guest-host" devices was switched on along with the concentration of doped TPE-PPE increased. With TPE-PPE fraction further increased, the light emission steadily intensified and PL peak appeared with no shift. As the concentration of luminescent TPE-PPE increased to 0.20 wt%, the optimal emission intensity at 535 nm was approximately 5.70-fold higher than that in 0.01 wt% TPE-PPE compositions. It was due to the different aggregate level derived from different concentrations of TPE-PPE in mesophases. In TPE-PPE, four mesogenic units are linked to a central olefin stator through single-bond axes, respectively. At low concentration of TPE-PPE in LC matrix, TPE-PPE molecules were almost isolated and would suffer from vibrant intramolecular rotations, leading to radiation-less relaxation of the excitons and emitting very weak light. However, along with the concentration of TPE-PPE in the viscous LC host was increased and the aggregation were formed,

the accompanying RIM and highly distorted molecular structures would hinder the intermolecular π-π stacking interaction of LCs. Therefore, higher concentrations of TPE-PPE were more conducive to overcome rotation barrier, which would bring a more efficient luminescence in LC states. While, the aggregation of fluorescein presented a rather noteworthy critical concentration quenching effect, resulting in the emission quenching of the luminophores in liquid crystal states. In a preliminary comparison, we utilized a prototypical fluorophore, fluorescein to study the AIE effects from the reverse side. Apparently, it could be noticed that the emission intensity of liquid crystal/fluorescein mixtures was intensively decreased when fluorescein, an ACQ dye, is progressively added into liquid crystal matrix. When the concentration of fluorescein rose to 0.20 wt%, the ACQ effects became visibly discriminable and the emission got exceedingly faint. In contrast to the RIR conformations of TPE-PPE, the rigid planar aromatic structures of fluorescein lead to π-π stacking interaction in liquid crystal phases. The excited states after absorbed energy would decay back to the ground states via non-radiative intermolecular energy transfer.

Table S1. Result of the quantum yield of the composites (SLC1717+0.2wt% TPE-PPE+Ag_2S), , related to Figure 2.

Ag_2S amount （wt%）	0	0.001	0.01	0.05	0.10	0.20
QY (quantum yield)	13.51%	14.00%	19.27%	27.09%	31.33%	38.22%

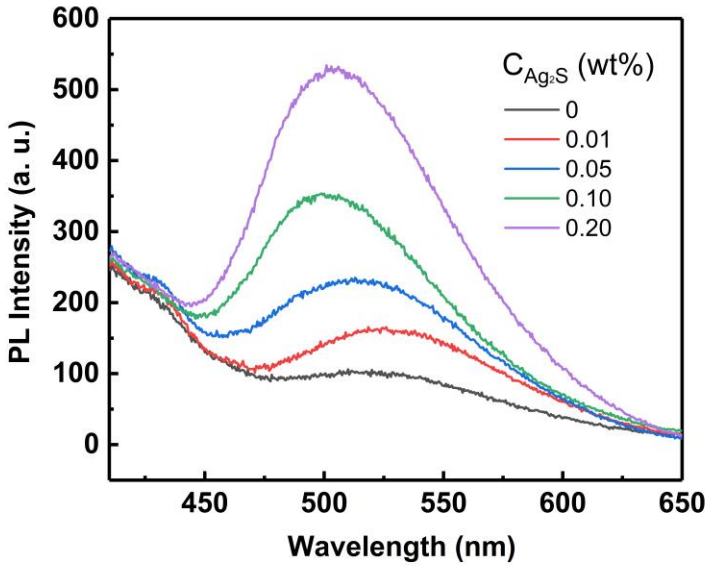

Figure S9. PL spectra of TPE-PPE (0.20 wt%) with different Ag_2S concentrations doping in glycerinum-THF solvent (v/v 1:1). Excitation wavelength: 340 nm, related to Figure 2.

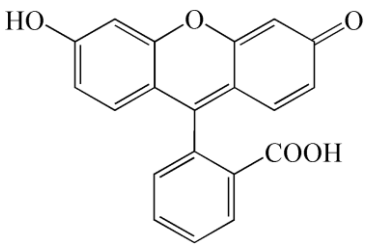

Figure S10. The chemical structure of fluorescein, which displayed a rigid planar aromatic structure, related to Figure 2 and 3.

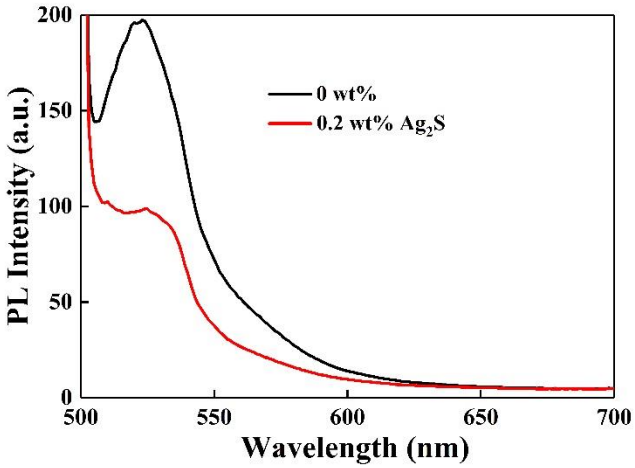

Figure S11. PL spectra of the sample SLC1717/fluorescein (100/0.20 wt%) composite doping Ag_2S with concentration of 0 and 0.20 wt%, related to Figure 2 and 3. Excitation wavelength: 489 nm.

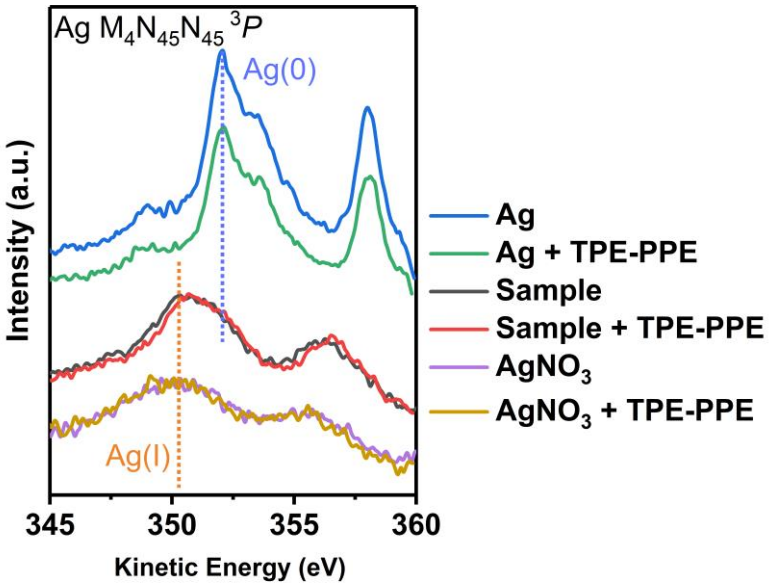

Figure S12. AES spectra of Ag $M_4N_{45}N_{45}$ Auger-electron line for amorphous Ag_2S micro-rods, crystal Ag, crystal $AgNO_3$ nanoparticles and their modified samples, related to Figure 1, 2 and 3. Compared with pure crystal Ag/$AgNO_3$ and TPE-PPE modified Ag/$AgNO_3$, Auger-electron line of Ag(I) parts of TPE-PPE modified amorphous Ag_2S micro-rods showed a tiny shift to the high kinetic energy. It means the conjugate electrons of TPE-PPE indeed partly transferred to the surficial Ag(I) irons, leading to a lower oxidation state and a lower binding energy of Ag(I).

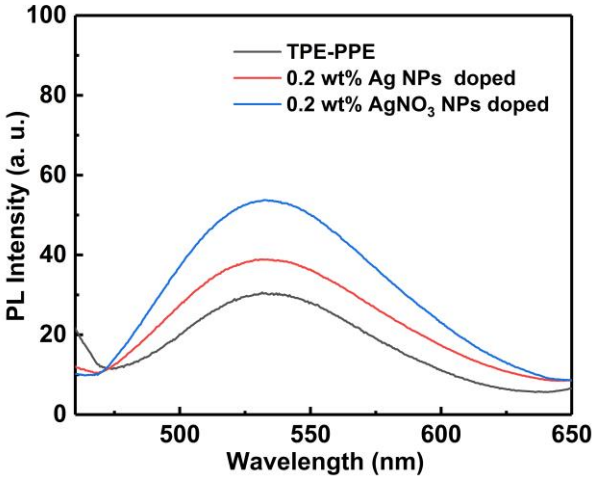

Figure S13. PL spectra of 0.20 wt% crystal Ag and $AgNO_3$ nanoparticles (NPs) doped into the SLC1717/TPE-PPE (100/0.20 wt%) composite, related to Figure 2 and 3. Compared with the original composite, the fluorescence enhancement of Ag and $AgNO_3$ NPs were much lower than amorphous Ag_2S micro-rods. Excitation wavelength: 340 nm.

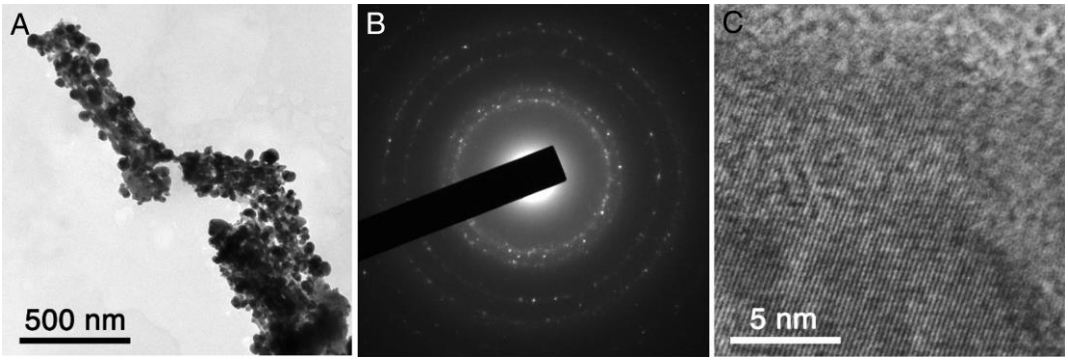

Figure S14. (A) TEM image, (B) SAED pattern and (C) HRTEM of the product under ultrasonic shaking for 3 h, related to Figure 4.

Table S2. Single point energies of the elements in the calculation by first principle calculation method, related to Figure 3 and 4.

	Single Point Energy (Kcal/mol)
Ag atom	$-9.186*10^4$
Ag (I) ion	$-9.169*10^4$
Ag_2S cluster	$-4.330*10^5$
Benzene ring	$-1.453*10^5$
Ag-benzene	$-2.371*10^5$
Ag (I)-benzene	$-2.498*10^5$
Ag_2S cluster-benzene	$-4.333*10^5$

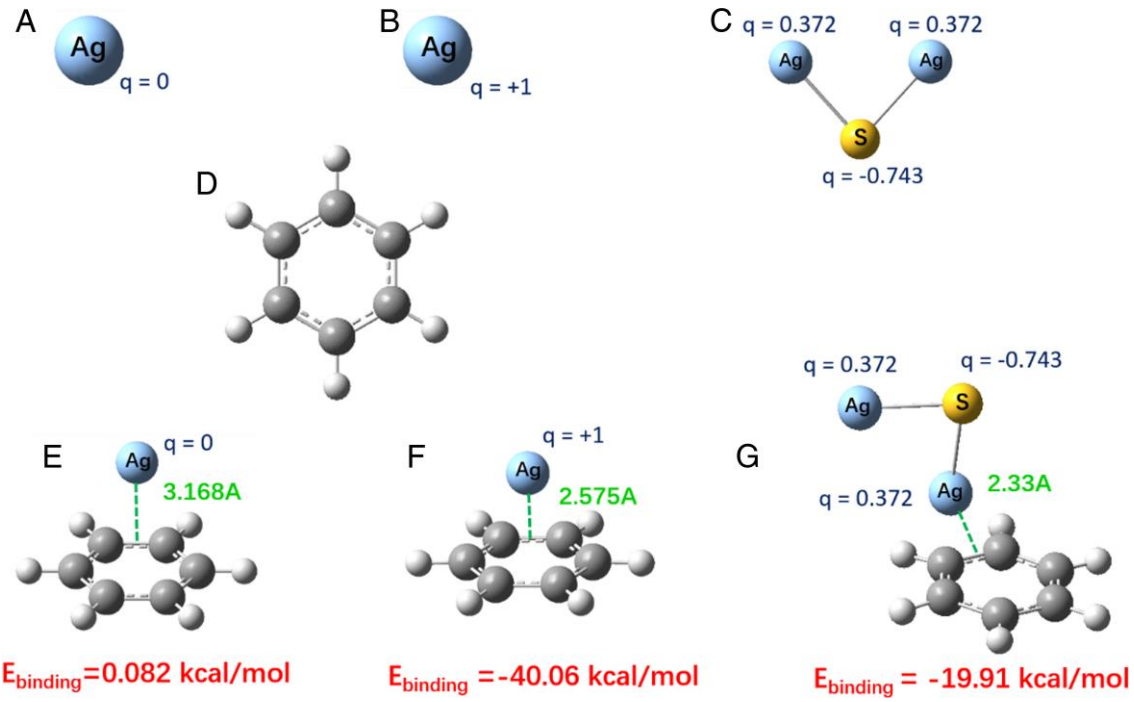

Figure S15. Structures of (A) Ag atom, (B) Ag (I) ion, (C) Ag_2S cluster, (D) phenyl and the binging energy of (E) Ag atom (F) Ag (I) ion and (G) Ag_2S cluster with the aromatic ring, related to Figure 3 and 4.

Transparent Methods

Materials: In this study, the positive nematic LC, SLC1717 ($\Delta n = 0.201$, $T_{NI} = 365$ K, $T_m = 233$ K) was purchased from Shijiazhuang Chengzhi Yonghua Display Material Co., Ltd and the polyvinyl alcohol (PVA) was from Alfa Aesar. The fluorescent dye, TPE-PPE was synthesized by a McMurry coupling and Sonogashira coupling, using the method of ref 13. The molecule structure is shown in Figure S6. All the chemicals used in the experiment were of analytical grade and without further purification.

Synthesis of amorphous Ag_2S hexagonal prisms: In a typical synthesis of the Ag complexes microrod, 4×10^{-5} mol sliver nitrate ($AgNO_3$) was first introduced into 30 mL dimethyl formamide (DMF) under constant stirring to obtain a homogeneous yellow solution at room temperature. Then the mixture was rapidly heated to 110 ℃. Afterwards, 10 mL dimethyl sulfoxide (DMSO) was added dropwise and held until lawn green precipitate emerged. After being cooled down to room temperature, the product was centrifuged and washed with ethanol for several times. Then the yellow product was redisposed in ethanol and treated under visible light irradiation for 10 min to decompose to amorphous Ag_2S hexagonal prisms.

Preparation of LC/TPE-PPE composites: In this experiment, the LC/TPE-PPE composites were prepared by integrating TPE-PPE dyes with the concentrations of 0.01 wt% to 0.20 wt% intensively dissolved in dichloromethane into the systems of the nematic LCs. Then the generating solutions were sonicated for about 5 min to achieve excellent solubility. After full evaporation of the dichloromethane solvent from the above solutions, the uniform LC/TPE-PPE compositions were obtained accordingly.

Preparation of LC/TPE-PPE/Ag_2S composites: By injecting the as-prepared Ag_2S micro-rods dispersed in ethanol solvent into above LC/TPE-PPE composites, the composites with different Ag_2S mass ratios of 0.01wt% to 0.20 wt% were obtained. In order to yield an admirable dispersion in the isotropy of SLC1717, the composites were sonicated for about 5 min at 95 ℃ and were cooled down to the anisotropic phase while vivaciously stirring. The process alleviated aggregation resulted from the nucleation of nematic domains and is a fantastically crucial factor of preparing stable dispersions of micromaterials in LC systems. Then the compositions were placed for 1 day to evaporate off residual ethanol completely, and finally, the LC/TPE-PPE compositions contained only one type of microparticles and no other additives.

Fabrication of LC cells: The inner surfaces of transparent indium-tin oxide (ITO) glass plates were coated with a 3.0 wt% polyvinyl alcohol (PVA) layer by spin-casting. Then the ensuing substrates were dried at 80 ℃ for 30 min and rubbed with a textile cloth to impose boundary conditions for LC director N. Two prepared substrates were fabricated in anti-parallel directions and glued together

containing 10 μm PET (polyethylene terephthalate) films. Eventually, the studied compositions were respectively infiltrated into LC cells by capillary action.

Characterization: The powder X-ray diffraction (XRD) of the Ag_2S was characterized by the Rigaku Rotaflex Dmax2200 diffractometer with Cu Kα radiation (λ = 1.54056 Å). The morphologies of Ag_2S MRs were observed using Hitachi S-4800 scanning electron microscopy (SEM) with an accelerating voltage of 10 kV. Transmission electron microscopy (TEM) and High-resolution transmission electron microscopy (HRTEM) images were recorded by JEOL JEM-2100F, with an accelerating voltage of 200 kV. Optical textures of composites were observed by a polarizing optical microscope (POM, Olympus BX51, Japan). The absorption spectra of Ag_2S were obtained with a Shimadzu UV-VIS spectrophotometer (UV-2600). Photoluminescence (PL) spectra were characterized using a Shimadzu RF-5301 Fluorescence Spectrometer. Quantum yield were measured by Edinburgh FLS980 Fluorescence Spectrometer with 450 W xenon lamp and integrating ball accessories.